Numerical modeling of flow processes over gravelly surfaces using structured grids and a numerical porosity treatment

S. N. Lane and R. J. Hardy

School of Geography, Faculty of Earth and Environment, University of Leeds, Leeds, UK

L. Elliott and D. B. Ingham

Centre for Computational Fluid Dynamics and Department of Applied Mathematics, University of Leeds, Leeds, UK

Received 20 December 2002; revised 9 July 2003; accepted 9 October 2003; published 8 January 2004.

[1] This article describes the development and validation of a method for representing the complex surface topography of gravel bed rivers in high-resolution three-dimensional computational fluid dynamic models. This is based on a regular structured grid and the application of a porosity modification to the mass conservation equation in which fully blocked cells are assigned a porosity of zero, fully unblocked cells are assigned a porosity of one, and partly blocked cells are assigned a porosity of between 0 and 1, according to the percentage of the cell volume that is blocked. The model retains an equilibrium wall function and an RNG-type two-equation turbulence model. The model is combined with a 0.002 m resolution digital elevation model of a flume-based, water-worked, gravel bed surface, acquired using two-media digital photogrammetry and with surface elevations that are precise to ±0.001 m. The model is validated by comparison with velocity data measured using a three-component acoustic Doppler velocimeter (ADV). Model validation demonstrates a significantly improved level of agreement than in previous studies, notably in relation to shear at the bed, although the resolution of model predictions was significantly higher than the ADV measurements, making model assessment in the presence of strong shear especially difficult. A series of simulations to assess model sensitivity to bed topographic and roughness representation were undertaken. These demonstrated inherent limitations in the prediction of 3-D flow fields in gravel bed rivers without high-resolution topographic representation. They also showed that model predictions of downstream flux were more sensitive to topographic smoothing that to changes in the roughness parameterization, reflecting the importance of both mass conservation (i.e., blockage) and momentum conservation effects at the grain and bed form scale. Model predictions allowed visualization of the structure of form-flow interactions at high resolution. In particular, the most protruding bed particles exerted a critical control on the turbulent kinetic energy maxima typically observed at about 20% of the flow depth above the bed. *INDEX TERMS:* 1815 Hydrology: Erosion and sedimentation; 1824 Hydrology: Geomorphology (1625); 1860 Hydrology: Runoff and streamflow; 1894 Hydrology: Instruments and techniques; *KEYWORDS:* CFD, gravel bed rivers, digital photogrammetry, roughness

Citation: Lane, S. N., R. J. Hardy, L. Elliott, and D. B. Ingham (2004), Numerical modeling of flow processes over gravelly surfaces using structured grids and a numerical porosity treatment, *Water Resour. Res.*, *40*, W01302, doi:10.1029/2002WR001934.

1. Introduction

[2] There is increased application of three-dimensional computational fluid dynamics to natural open channel flows, often over quite complex topographies [e.g., *Hodskinson and Ferguson*, 1998; *Sinha et al.*, 1998; *Gessler et al.*, 1999; *Nicholas and Sambrook-Smith*, 1999; *Bradbrook et al.*, 2000; *Wu et al.*, 2000; *Booker et al.*, 2001]. The interest in doing this stems from a number of reasons. First, research has shown [e.g., *Lane et al.*, 2000] that using point measurements of flow velocity to infer reach-scale channel flow processes in 3-D can be misleading. Numerical modeling in 3-D has appeal in this respect. However, both *Dietrich* [1987] and *Bradbrook et al.* [2000] show that there can be significant deviation between the results of both experimental and numerical modeling studies of idealized river channels (commonly with rectangular or trapezoidal cross sections) and those of real rivers. Much of this relates to the role of topographic forcing, where within-channel topographic variability in both the downstream and cross-stream direction can be as influential as or dominate over other terms in a classical force balance analysis [e.g., *Dietrich*, 1987]. Thus understanding the influence of complex topography upon flow processes is a crucial goal, and three-dimensional modeling using a full topographic representation is a way forward. Second, this topographic forcing has important

0043-1397/04/2002WR001934$09.00

implications for the nature of sediment transport and river channel change [e.g., *Dietrich*, 1987]. *Bradbrook et al.* [2000] show how scour at tributary junctions results in strong downwelling, and hence transfer of momentum toward the bed, assisting in the maintenance of channel scour. However, in the absence of scour, numerical simulations suggested that downwelling was significantly reduced, causing us to explore different explanations for scour hole formation. The richness of the three-dimensional flow field associated with three-dimensional numerical modeling, along with the ability to simulate interactions between different bed topographies and flows [e.g., *Bradbrook et al.*, 2001], allows testing of a much wider range of hypotheses over the interaction between river channel form and process. Third, it is clear that the three-dimensional flow structure of rivers, especially gravel bed rivers exerts a crucial control upon habitat, and its spatial variation. *Leclerc et al.* [1995, 1996] demonstrate that 2-D hydraulic modeling allowed a much better match between the spatial scale of salmonid function and hydraulic predictions. *Crowder and Diplas* [2000] showed that point measurements of habitat did not represent habitat variation in space by using a model that included mesoscale topographic features (e.g., boulders). By scaling the spatial change in kinetic energy between two points by the kinetic energy at the point with the smaller velocity, they were able to derive a metric that represents the kinetic energy that must be spent by an organism in order to move from the point of lower velocity to the point of higher velocity. The presence of boulders resulted in a substantially more complex spatial metric which provided a greater habitat range for fish. Linking this to observed fish behavior [*Crowder and Diplas*, 2002] confirmed that boulders enhanced the potential availability of the right habitat. Again, obtaining information on the full three-dimensional flow field allows us to start to understand the interaction between habitat and flow hydraulics and so develop much more sophisticated analysis of the parameters that describe habitat availability and their change through time.

[3] Given the potential of using three-dimensional applications of computational fluid dynamics to explore fluvial flows and the demonstrated achievement of this method in certain application areas, this paper seeks to address a fundamental methodological problem that has yet to be addressed. Research into the performance of numerical code is emphasizing, amongst other things, the need for careful investigation of numerical diffusion associated with grid specification, the accuracy of discretization [e.g., *Manson and Wallis*, 1997], and convergence problems associated with fine grids in finite volume discretizations [e.g., *Cornelius et al.*, 1999]. Provided attention is given to the way in which the numerical solution achieves convergence [*Cornelius et al.*, 1999], finite volume treatments using structured grids have particular appeal as they provide a fast and efficient numerical solution and can be numerically stable in channels of simple geometry. However, two problems emerge. First, in channels of more complex geometry, where boundary-fitted coordinates must be used, they are much less stable and numerical diffusion can be high. Second, for coupling to sediment transport treatments, erosion or deposition (in a 3-D model) requires an adaptive gridding capability. Mesh generation and re-generation associated with this is a particular problem if lateral channel change is involved [*Lane*, 1998]. The aims of this paper are (1) to develop a method identified by *Olsen and Stokseth* [1995] for representing complex topography in regular structured grids using a porosity treatment; (2) to combine this method with high-resolution topographic data for a real water-worked gravel bed surface; and (3) to validate model predictions using point measurements obtained using acoustic Doppler velocimetry.

2. Background to Approach

[4] The traditional approach to the treatment of channels with complex geometry involves fitting a mesh to available topographic data and then parameterizing smaller scale aspects of topography using a roughness parameter [e.g., *Hodskinson and Ferguson*, 1998; *Nicholas and Sambrook-Smith*, 1999; *Lane et al.*, 1999]. In the latter, the skin friction associated with grain surfaces, as represented through a roughness height, is multiplied upward [e.g., *Clifford et al.*, 1992]. Thus the effects of subgrid-scale topography (e.g., grain surface morphology, grain interactions) are represented as frictional retardation of the flow at the bed. This is normally based upon a standard "law of the wall":

$$\frac{u}{u_*} = \frac{1}{\kappa} \ln\left(\frac{z}{z_o}\right) \tag{1}$$

where u is the flow magnitude in the planform direction; z is elevation above a reference plane; u_* is the shear velocity = $\sqrt{\tau_b/\rho}$; κ is the Von Karman constant (=0.4); τ_b is the bed shear stress; ρ is the fluid density; and z_o is the height of zero velocity, which depends on the bed roughness. Bed roughness may be defined from the following:

$$z_o = \frac{\upsilon}{9u_*}, \tag{2a}$$

for smooth boundaries and

$$z_o = \frac{1}{30} ks \tag{2b}$$

for rough boundaries, where υ is the kinematic viscosity; and k_s is the equivalent sand roughness following *Nikuradse* [1933]. In practice, equation (1) is modified as it assumes local equilibrium of turbulence, which is violated under conditions of flow separation. Thus *Launder and Spalding* [1974] recommend a nonequilibrium law-of-the-wall in which shear velocity is replaced by the square root of the turbulent kinetic energy per unit mass (k) as the characteristic velocity scale:

$$\frac{u\sqrt{k}}{u_*^2} = \frac{\ln\left(0.25c'_\mu \frac{\sqrt{k}}{u_*}\frac{z}{z_o}\right)}{0.25c'_\mu\kappa} \tag{3}$$

where c'_μ is an empirically derived coefficient equal to 0.09 [*Launder and Spalding*, 1974]. In theory, provided the mesh is designed properly at the boundary, such that equation (3)

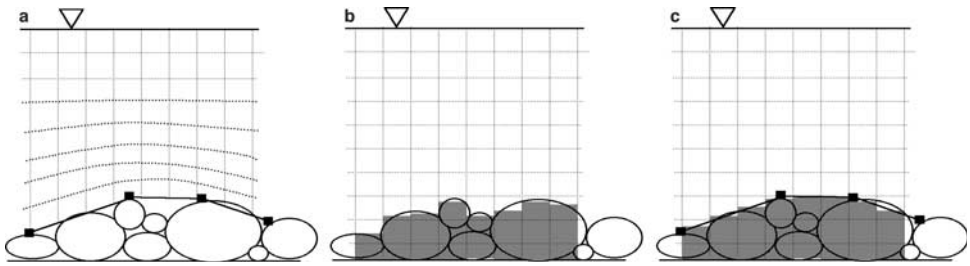

Figure 1. (a) Boundary fitted coordinates applied to sampled topographic data; (b) topographic representation using a porosity treatment with high-resolution topographic data; (c) topographic representation using a porosity treatment with sampled topographic data; for an idealized, rough, gravel bed surface. Solid squares represent field sampled data points.

is only applied to boundary cells and the boundary is smooth, the main concern becomes the validity of the turbulence model. In practice, k may be determined from the transport equations in a two-equation turbulence model, with diffusion of energy to the wall assumed to be zero, production expressed in terms of the shear velocity ($u_*^2 u/2z$) and the boundary condition for turbulent energy dissipation (ε) set as:

$$\varepsilon = \frac{\left(c'_\mu\right)^{3/4} k^{3/2} \ln\left(0.25 c'_\mu \frac{\sqrt{k}}{u_*}\frac{z}{z_o}\right)}{2ky} \tag{4}$$

If the condition for local equilibrium applies, equation (4) reduces to equation (1).

[5] While there are significant concerns over turbulence parameterization in these near wall treatments, research has demonstrated that, in natural river channels with gravelly beds, much greater uncertainty is introduced into predictions of the three-dimensional velocity field due to poor knowledge and treatment of topographic variability than is introduced by uncertainty over turbulence treatments at the wall [*Lane et al.*, 1999]. The basic principle adopted for representing topographic variability involves the multiplication upward of the equivalent sand grain roughness (k_s) in equation (2b). In a 3-D modeling framework, this assumes that the topographic variability that is not included in the model geometry is represented as a subgrid scale effect through upscaling of z_o used in equation (2b). Much of this uncertainty relates to debate over which grain parameter to upscale and by how much. For instance, field investigations suggest that z_o should, including upscaling, take a value of approximately $0.1D_{84}$ [*Whiting and Dietrich*, 1990; *Wiberg and Smith*, 1991]. Others, specifying it as k_s (noting $k_s = 30z_o$), have suggested approximately $3.5D_{84}$ or $6.8D_{50}$ [*Hey*, 1979; *Bray*, 1982]. *Clifford et al.* [1992] show that multiplication of roughness length represents a measure of total flow resistance that incorporates contributions from both individual grains and larger bed forms.

[6] These uncertainties aside, the z_o approach is associated with a number of problems. First, a wide range of grain percentiles have been adopted. While there is a general preference for the D_{84} [e.g., *Whiting and Dietrich*, 1990; *Wiberg and Smith*, 1991] the most appropriate percentile may depend upon the size distribution and sorting of the gravel mix. Second, for modeling purposes, the multiplier of roughness length will need to be spatially variable and scale dependent, in relation to both mesh resolution and the topographic content of the data set used to describe the surface. Third, some studies have noted problems in terms of numerical stability and solution accuracy for flows characterized by high relative roughness [e.g., *Nicholas and Sambrook-Smith*, 1999] with these difficulties resulting from the existence of an upper limit of k_s for a given near-bed cell thickness [*Nicholas*, 2001]. The implication of this is that the thickness of the near bed cell limits the maximum shear velocity at the bed, so that near bed velocities may be over predicted in field situations that involve high relative roughness [*Nicholas*, 2001]. Fourth, there is the basic problem of setting the reference height of the bed in a numerical mesh: normally, it is assumed implicitly that the effective bed surface in mass conservation terms is the same as the bed surface sampled during field survey. Figure 1a shows how blocked grid cells are not effectively blocked in a boundary fitted coordinate treatment. Even if the drag term can be effectively specified, there will be mass conservation errors arising from cells that are not blocked but which should be; and cells that are blocked that should not be. It also demonstrates the real uncertainty in the value that the multiplier of roughness length should take. The grid cells in Figure 1a are smaller than the average topographic spacing. Thus the multiplier effect has to represent both subgrid-scale topographic roughness and a roughness component that is lost because of the coarse spacing of topographic data collection. This suggests implicit limits to the use of a roughness parameter such as z_o to represent topographic effects in three-dimensional flow models.

[7] In practice, the problems in Figure 1a arise from the coarse sampling of topographic data. The main alternative to using a multiplier of roughness length is to begin to include topographic data in the model. If actual data is available, then roughness due to a difference between sampling density and grid density may be represented through introduction of topographic variability into the boundary fitted coordinates. For instance, *Nicholas* [2001] attempted to include bed form roughness (e.g., particle clusters) by using a random elevation model to introduce topographic variability into the CFD mesh. This reduces the roughness problem to subgrid-scale topographic variability, but assumes that (1) the random elevation model provides an adequate representation of topography; and (2) the mesh distortion that arises from using the boundary-fitted coordinate approach does not affect the numerical solution.

[8] This paper makes progress with these assumptions in two respects. First, developments in through-water (two media) photogrammetry have proved capable of generat-

ing accurate and precise (±0.0005 m), high-resolution (0.001 m grid spacing) digital elevation models (DEMs) of submerged gravels for both field [*Butler et al.*, 2002] and flume [*Butler et al.*, 1998, 2002; *Lane*, 2001] situations. Second, research into the performance of numerical code has emphasized, amongst other things, the need for careful investigation of discretization. This includes the accuracy of discretization [e.g., *Manson and Wallis*, 1997], convergence problems associated with fine grids in finite volume discretizations [e.g., *Cornelius et al.*, 1999] and the spatial discretization required for verification [*Hardy et al.*, 2003]. However, provided attention is given to the way in which numerical solution achieves convergence [*Cornelius et al.*, 1999], finite volume treatments using structured grids have particular appeal as they provide fast and efficient numerical solution and can be numerically stable in channels of simple geometry. Stability problems may arise in channels of more complex geometry, where body-fitted coordinates must be used. When meshes are fitted to the irregular bottom topography of natural river channels, there may be marked spatial variation in grid size that may confound attempts to achieve grid-independent solutions and also result in significant numerical diffusion. Therefore there is a need to develop finite volume schemes that can represent complex topographies without distorting the grid cell size. Hence we deal with this problem by developing the approach of *Olsen and Stokseth* [1995], which retains the use of a structured grid but specifies cell porosities to block out bottom topography (Figure 1b). We extend this approach to scale the drag terms required by the introduction of the porosity approach. We are able to make use of a unique data set that combines high-quality two-media digital photogrammetric topographic data [from *Butler et al.*, 2002] with a dense network of three-dimensional flow measurements over the same surface.

3. Numerical Scheme and Experimental Design

[9] The numerical scheme involves a finite volume solution of the full three-dimensional Navier-Stokes equations in a Cartesian coordinate system, with a Renormalized Group Theory (RNG) k-ε turbulence model.

3.1. Porosity Treatment and Modification of Drag Terms

[10] The porosity treatment is based upon the *Olsen and Stokseth* [1995] approach, and we extend their methodology to modify the drag terms introduced due to the porosity treatment. For a given Cartesian mesh, the topography is transformed into porosity values within the mesh. In this situation, we assume that the topographic data takes the form of a DEM, with a density of topographic data equal to (Figure 1b) or greater than the grid density. We also assume that the numerical grid is defined with vertices that are exactly collocated to the DEM. This means that either: (1) the DEM elevations map directly onto grid cells (equal density); or (2) the grid cells each contain a unique set of DEM elevations (greater topographic density), which can be used to determine the average elevation. In the latter case, with a regular grid, there is a geometric series of possible DEM elevations in a given grid cell (i.e., 1, 4, 9, 16, 25, 36. . ..).

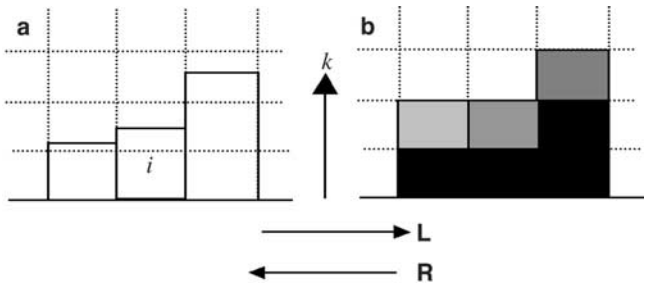

Figure 2. Illustration of the flow direction dependence of the scaling term for drag. (a) DEM elevations. (b) DEM elevations after porosity determination with solid areas for $P_{ijk} = 0$, open areas for $P_{ijk} = 1$; and shaded areas indicating $0 < P_{ijk} < 1$.

[11] These two situations need slightly different treatments in terms of porosity. Consider a structured, orthogonal Cartesian grid with directions i and j in the planform and k in the vertical. The equal density case is simplest, as each porosity value (P_{ijk}) can be defined for each column of data at planform location (i, j), which has a singular value of elevation, E_{ij}. Thus for cell k, if Z_{ijk} is the center of the cell and we assume cuboid cells so that the thickness of the cell (ΔZ_{ij}) is the same throughout the column, then there are three rules:

$$E_{ij} \geq Z_{ijk} + 0.5\Delta Z_{ij}, \quad P_{ijk} = 0 \tag{5a}$$

$$Z_{ijk} - 0.5\Delta Z_{ij} < E_{ij} < Z_{ijk} + 0.5\Delta Z_{ij}, \quad P_{ijk} = \left[\frac{(E_{ij} - Z_{ijk})}{\Delta Z_{ij}} + 0.5\right] \tag{5b}$$

$$E_{ij} \leq Z_{ijk} - 0.5\Delta Z_{ij}, \quad P_{ijk} = 1 \tag{5c}$$

For the second case, there are a number of solutions of varying complexity. The simplest is based upon deriving the average elevation for a given grid cell from the DEM values within that grid cell. However, if there are 9 (i.e., a 3 by 3 elevation matrix) or more elevations being assigned to a single grid cell, it is possible to determine a more realistic value of porosity by fitting surfaces to the elevation matrix and then working out the area-integrated average elevation as the basis of the porosity value.

[12] Following *Olsen and Stokseth* [1995], and noting the observation that, for rough gravelly surfaces, dealing with the effects of topography upon mass conservation should be a prime concern, we assume that the source term represented by the drag terms in the momentum equation is so great that it dominates over the turbulent diffusion terms. Thus the values of k and ε in the porous domain (for $0 < P < 1$) will have only negligible effects on the flow field and the standard RNG theory k-ε turbulence model is not modified in these cells. Thus the only modification to the momentum equations that is required is a scaling of the drag term derived from the law-of-the-wall to represent the effective exposed area of the surface. To do this, we recognize that the effective drag on an element will depend upon the direction of flow. Considering a simple two-dimensional case (Figure 2a), the

effective drag experienced by cell i with flow direction L is greater than with direction R.

[13] There are three levels of complexity here that, as with the porosity specification, need to be considered in relation to both the DEM resolution and the grid resolution. In the ideal case, the DEM resolution is such that it contains all scales of topographic variation other than the grain surface scale [*Butler et al.*, 2002] and the mesh resolution is the same as the surface resolution. For this, with a first approximation of flow direction, we augment the drag exerted by a given cell according to the change in porosity in the flow direction. For a given cell, the four differences in porosity between cell (i, j) and cells $(i - 1, j)$, $(i + 1, j)$, $(i, j - 1)$ and $(i, j + 1)$ are calculated. If there is a component of flow out of the cell in the + or − i-direction or + or − j-direction and porosity decreases in that direction (i.e., the adjacent cell has a higher elevation) then there is an effective "jump" and the drag coefficient must be scaled accordingly. Otherwise, no scaling is applied. The scaling is based upon the effective (equivalent) surface area. We assume that all drag is exerted along the base of cells other than for the sidewalls of the channel. A surface is then fitted to the 3 by 3 matrix of elevations centered on cell (i, j). The area (a_{ij}) of this surface for cell (i, j) can then be determined for the four vertices of the cell: $(i + 0.5\Delta X_{ij}, j + 0.5\Delta Y_{ij})$; $(i + 0.5\Delta X_{ij}, j - 0.5\Delta Y_{ij})$; $(i - 0.5\Delta X_{ij}, j - 0.5\Delta Y_{ij})$; and $(i - 0.5\Delta X_{ij}, j + 0.5\Delta Y_{ij})$; where ΔX_{ij} is the grid resolution in the i direction for cell (i, j) and ΔY_{ij} is the grid resolution in the j direction for cell (i, j). With cuboid grids, $\Delta X_{ij} = \Delta Y_{ij} = \Delta Z_{ij}$ and the scaling factor (s_{ij}) is then applied to the roughness height in the wall function using:

$$s_{ij} = \frac{a_{ij}}{\Delta Z_{ij}^2} \tag{6}$$

We believe that equation (6) provides a good conceptual representation of the drag augmentation: increasing the roughness height increases the effective elevation at which the planform component of velocity would become zero. Although we are now scaling roughness height in a manner that we sought to avoid, it is important to recognize that this is now only being applied to the grain surface scale and the total contribution of the drag term defined by the law of the wall should be significantly smaller as larger scales of topography are represented explicitly in the numerical mesh. We explore sensitivity to z_o with the porosity treatment below.

[14] In the second case, the DEM is of a higher resolution than the mesh. In this case, there is information on subgrid-scale topographic variability available from the DEM. In theory, this could be represented by an increase in the roughness height, which would be some function of the standard deviation of DEM elevations falling within each boundary cell. However, *Nicholas* [2001] shows that the magnitude of the required roughness height is related to both topographic resolution and mesh resolution, the latter because of the way in which fluid shear between adjacent grid cells is resolved. Thus there will be a nonlinear relationship between any roughness parameter and the required mesh resolution, of a form that has yet to be fully investigated. This special case is therefore not considered here.

[15] In the third case, the DEM is of a coarser resolution than the mesh. This is typically the case in applications of CFD to natural channels and traditionally requires specification of a roughness parameter to represent the effects of this subgrid-scale topography. The porosity model provides an alternative method for dealing with this problem. Provided something is known about the subgrid-scale variability (e.g., the surface fractal dimension [*Butler et al.*, 2001]), then this can be used to create local topographic variability through the porosity field. As with the case where the DEM resolution matches the mesh resolution, this means that the roughness height only needs to be specified at the scale of the mesh.

3.2. Boundary Conditions

[16] Boundary conditions need to be specified at the upstream inlet and downstream outlet, at the sidewalls and at the free surface. The upstream inlet is specified from experimental data (see below) and the downstream outlet is specified as a fully developed flow profile with the hydrostatic pressure set at the surface at the downstream outlet. The standard RNG theory k-ε turbulence model is not modified at the sidewalls or the bed and the equilibrium wall function is used. A roughness height (z_o) is specified. For the standard turbulence model to be valid, the z^+ criterion must be satisfied:

$$30 < z^+ < 300 \tag{7}$$

where

$$z^+ = \frac{\sqrt{\tau_b/\rho}}{\upsilon} z_b$$

and τ_b is the bed shear stress; υ is the kinematic viscosity; and z_b is the distance of the center of the wall adjacent cell from the wall which, for the case of cuboid cells, is $\Delta Z_{ij}/2$. This allows us to make sure that the first grid cell lies within the wall region and outside of the laminar sublayer. Within the wall region, shear within the fluid can be assumed to be the same as shear at the bed, and determined using the equilibrium form of the law of the wall [*Prandtl*, 1952].

[17] At the free surface, we use a method applied by *Bradbrook et al.* [2000]. This uses a symmetry plane at the surface across which all normal resolutes are set to zero. To represent the effects of water surface variation, nonzero pressure terms on the symmetry plane are introduced to the momentum equations, commonly referred to as a rigid-lid treatment. This allows for the effects of both water surface superelevation and depression with respect to the plane in terms of the momentum equations. However, if the mass conservation equations are not corrected, it will lead to under estimation of velocities in zones of water surface depression and over estimation of velocities in zones of water surface superelevation. To deal with this, we introduce an effective surface cell thickness (ΔZ_{sij}) into the continuity equation, which scales the equivalent cell face area in the cross-stream and downstream directions according to the pressure (P_{sij}) on the symmetry plane at cell (i, j):

$$\Delta Z_{sij} = \left(\frac{P_{sij} - \rho g h_{cij}}{\rho g h_{cij}}\right) + \Delta Z_{ij} \tag{8}$$

where h_{cij} is the elevation of the surface grid cell at location (i, j). *Bradbrook et al.* [2000] show that this yields a stable approximation of free surface elevation provided spatial gradients of water surface are not too great, and normally not greater than ΔZ_{ij}. This case is evaluated with each application of the model.

3.3. Numerical Solution

[18] Numerical solution is based upon a finite volume approach. The use of a regular, structured mesh means that the Cartesian space is essentially the same as the computational space. The following nomenclature is used: C is the cell center; P is the present time step; N, S, E, W, H, L are the centers of neighboring cells; E to W is increasing i direction; S to N is increasing j direction; H to L is increasing k direction; and T is the cell center at previous time step. Thus the mass conservation equation integrated over a cell volume is:

$$a_P f_P = a_N f_N + a_S f_S + a_E f_E + a_W f_W + a_H f_H + a_L f_L + a_T f_T + \text{source terms} \quad (9)$$

where f is a variable and a is the neighboring link across a cell face:

$$a = Au\rho + \frac{AG_f}{\Delta x} + \frac{V\rho}{\Delta t} \quad (10)$$

where: A is the cell face area; u is the velocity component perpendicular to the face; V is the cell volume; G_f is the diffusive exchange coefficient for f; Δx is the distance between cell centers which equals ΔZ_{ij} in a cuboid grid; and Δt = time step. The cell center coefficient is given by continuity:

$$a_P = a_N + a_S + a_E + a_W + a_H + a_L + a_T \quad (11)$$

During solution, the finite volume equation is used to correct coefficients with the aim that errors converge on zero as the solution proceeds.

[19] Scalar quantities are stored at cell centers and vector quantities at the centers of cell faces. Interpolation assumptions must be made to obtain scalar values at cell faces and vector values at cell centers. If the convective (J) and diffusive (D) parts of the flux across a face are separated then equation (9) can be written as

$$J_N - J_S + J_E - J_W + J_H - J_L + D_N - D_S + D_E - D_W + D_H - D_L = S_p \quad (12)$$

where S_p is the source and transient terms. Convection fluxes through cell faces are defined as

$$J = Cf \quad (13)$$

where C is the mass flow rate across the cell face. Interpolation to cell face values is based upon a Hybrid-Differencing Scheme (HDS). A Cell Peclet number is defined as

$$Pe = \rho|u|\frac{A}{D} \quad (14)$$

If $Pe > 2$, an upwind differencing scheme is used which assumes that the convected variable at the cell face is the same as the upwind cell center. This is highly stable, but only first order accurate, and so highly diffusive when flow direction is skewed relative to gridlines. As we are using regular structured meshes in this case, this problem is significantly reduced. If $Pe < 2$, diffusion dominates and a second order Central Differencing Scheme is used.

[20] To couple the mass conservation and momentum equations, the SIMPLEST algorithm is used (based on the work of *Patankar and Spalding* [1972]). This (1) takes an initial estimate of the pressure field to solve the momentum equation; (2) determines the consequent mass conservation errors; (3) solves a pressure correction equation; (4) adjusts the pressure and velocity fields; and then (5) applies this corrected pressure to the momentum equation. This is repeated until the mass conservation and momentum errors are acceptably small. This convergence can proceed either smoothly or with damped oscillations to the final solution. To achieve relaxation either: (1) realistic maximum and minimum values may be imposed on the solution; or (2) relaxation may be used to limit the amount of change allowed in any variable at a given iteration. Weak linear relaxation was used for the pressure correction and weak false time step relaxation was used for the other variables. The convergence criterion was set such that mass and momentum flux residuals were reduced to 0.1% of the inlet flux.

[21] The porosity treatment was introduced in a series of stages. First, an initial solution was obtained for the flat bed case. Second, the porosity treatment without the drag terms was introduced. Finally, the drag terms were applied iteratively until there was negligible change in drag.

3.4. Experimental Design: Laboratory

[22] The experimental geometry used for model development and validation is based upon water worked gravels in a 0.30 m wide and 8.0 m long tilting flume. A bulk sample of sediment from the River Affric, Scotland was placed in the flume (D_{50} = 0.020 m; D_{84} = 0.069 m) and water worked until a stable bed (no sediment transport) with a realistic structure was obtained with a flow depth of approximately 0.240 m. This realism was established using scaling analysis [*Butler et al.*, 2001] and shown to have expected morphological characteristics: isotropic scaling at the grain surface scale; anisotropic scaling, oriented toward the predominant flow direction, at the grain-scale; and grain organization into small bed form like structures. Table 1 summarizes the hydraulic conditions used in the study and Figure 3 shows a vertical view of the gravels.

[23] Once the gravels had been water worked, the surface morphology (e.g., Figure 3) was measured using two-media digital photogrammetry (see *Butler et al.* [2002] for full explanation). In summary, a transparent Perspex sheet (0.003 m thick) was used to flatten the water surface at the time of exposure and five photogrammetric targets were fixed on the upper surface of the Perspex. DEM generation was based upon 1:15 scale panchromatic stereo-photographs, acquired using two semi-metric Hasselblad ELX cameras, supported on a specially designed movable gantry. The cameras were mounted 1.2 m above the bed and separated by 0.31 m. Such geometry provided approximately 65% overlap between the images, with a base: distance ratio

Table 1. Basic Hydraulic Data Associated With the Flume Experiments

Parameter	Experimental Value
Average flow depth (m)	0.225
Maximum flow depth (m)	0.240
Width (m)	0.300
Discharge (m^3s^{-1})	0.0216
Flow Reynolds number	2.88×10^4
Froude number	0.215
Sediment D_{50} (m)	0.020
Sediment D_{84} (m)	0.069

of approximately 1:4, which met general precision requirements (theoretical height estimation to within ±0.001 m). The use of three exposure stations provided continuous coverage of a 1 m strip of exposed flume bed (Figure 4). The approximate focal lengths of the cameras were 0.08 m, and this parameter and an appropriate lens model were determined using self-calibrating bundle adjustment methods as explained by *Chandler et al.* [2001]. This experimental set-up allowed generation of DEMs at a spacing of 0.001 m. These DEMs have been subject to intensive data quality tests, in terms of point precision and accuracy and surface precision and accuracy [e.g., *Butler et al.*, 1998, 2001, 2002]. For the topography shown in Figure 4 the mean surface error was 0.0008 m and the standard deviation of error was ±0.0017 m. The latter was somewhat degraded from the theoretical precision of ±0.001 m, but only 8.5% of the grain-size D_{50}, and so assumed to provide excellent topographic representation. The main area where this topographic representation will be less effective will be areas of dead ground [*Butler et al.*, 1998], in the crevices between individual grains.

[24] For the purpose of setting inlet boundary conditions and for model validation, velocity profiles were collected with a NorTek® Acoustic Doppler Velocimeter (ADV) measuring 0.010 m intervals above the bed at the planform locations shown in Figure 5. The ADV was mounted on a carriage set on the flume sidewalls and oriented into the same coordinate system used to define the bed topography, with x velocities in the ADV set to be parallel to the x direction in the DEM. In planform, three strips of data were collected, one along the flume centerline and two either side of the centerline, each shifted by 0.050 m. In addition, for three locations in the downstream direction, an extra two velocity profiles were measured to assist in the specification of inlet conditions (Figure 5). Data were collected at 25 Hz for 120 s and subject to the basic screening recommended by *Lane et al.* [1998]: the focus of this study was mean flow velocities and low order turbulence parameters and so filtering of each time series to remove noise was limited to the removal of data points with insufficient signal-to-noise ratios and point correlations less than 0.7 [*Lane et al.*, 1998].

3.5. Model Geometry and Boundary Conditions

[25] For the purpose of these experiments, a 0.70 m long and 0.20 m wide section of river bed gravel was used to define the bed geometry. The computational domain was regular in the xy and z directions, with a grid resolution of 0.002 m. In the z direction, to allow inclusion of topography data using the porosity treatment, the maximum extent of the domain was set at 0.24 m. Thus the computational grid was sized at 350 by 110 by 120 (4 620 000 grid cells). In both, the topography data was transformed into porosity data. In this case, there were 4 DEM elevations available for each cell in the numerical mesh and hence the porosity was set according to the average of these elevations. At the upstream inlet, inlet conditions were specified using the ADV data for cross section 1, as shown in Figure 6.

[26] As we consider below, there ought to be very low sensitivity to roughness height specification given that the majority of the topographic variability is now specified explicitly. However, the wall treatment in the model still requires specification of a roughness height. Given the DEM and grid resolution (0.002 m), and the DEM precision (±0.0017 m [*Butler et al.*, 1998]), the model will provide an explicit first order representation of topographic scales greater than 0.004 m (i.e., following the Nyquist rule that the lowest detectable periodicity is twice the sampling interval). The roughness height needs to parameterize the scales that are smaller than this. As we are now dealing with grain surfaces, rather than grain organizations (as in equation (2b)) we set the roughness height at 0.001 m (50% of the resolved scales) to reflect the probable sub grid-scale topographic representation associated with the model. It should be emphasized that (1) there are no a priori experiments that have dealt with this scale of topographic data (as opposed to grain-size data) in a hydraulic model of this kind; and (2) in theory, the model should be very insensitive to specification of z_o. If this low sensitivity can be demonstrated (see below) we have removed one of the major uncertainties in modeling flows in 3-D over gravely surfaces: a strong dependence upon roughness height specification.

3.6. Model Validation

[27] Model validation used an automated correspondence algorithm to match ADV measurement locations to

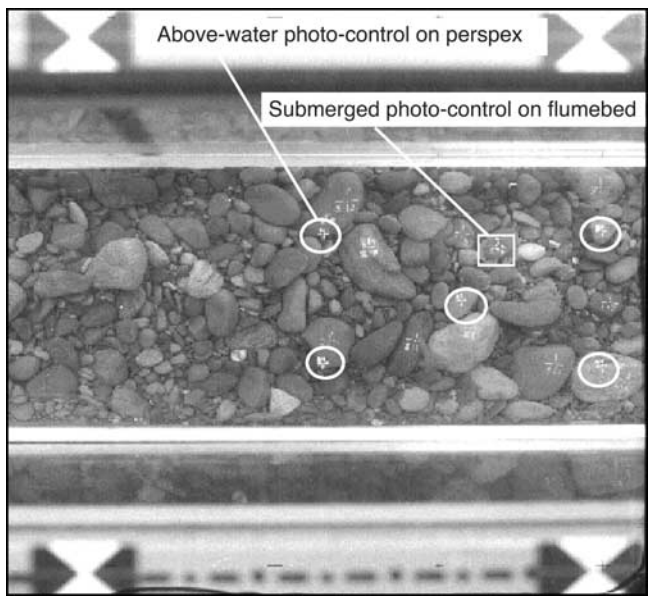

Figure 3. A vertical view of the water-worked gravels. This shows the photocontrol used for the photogrammetry. Flow measurements were surveyed into the same coordinate system used for the photogrammetry to allow a direct match up with model predictions.

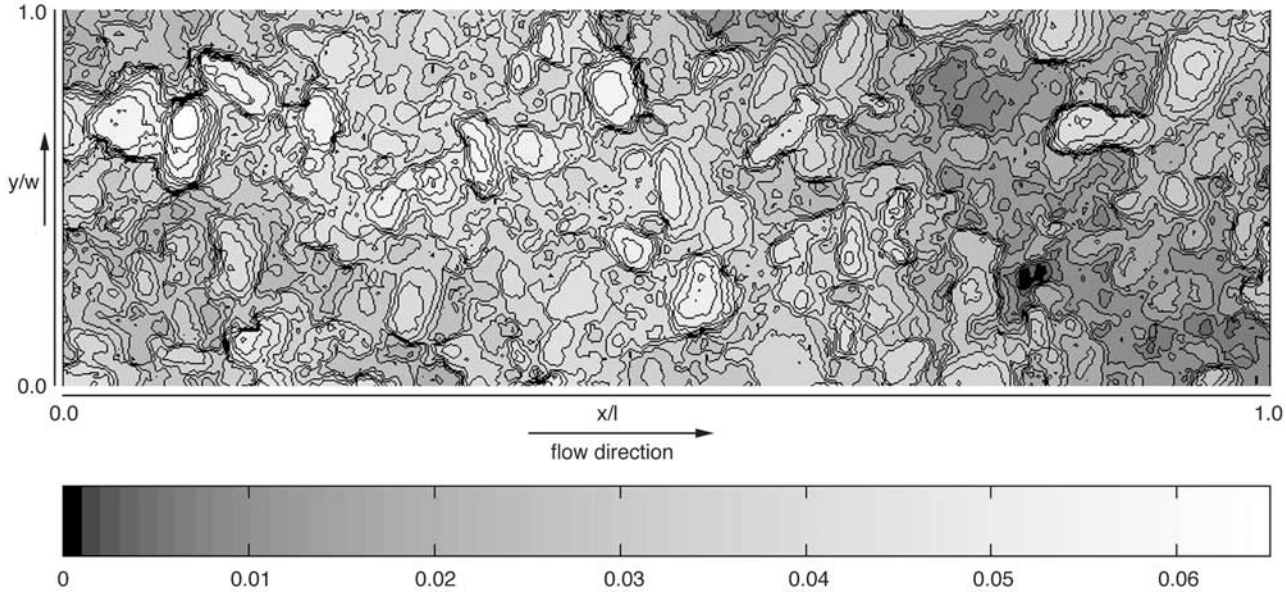

Figure 4. DEM of the flume bed used in this study.

corresponding grid cell locations. The size of the model grid cells was 0.002 m by 0.002 m by 0.002 m. The ADV measures in a 0.08 m diameter cylindrical sampling volume, with a height of 0.010 m. Thus it determines a spatially averaged velocity that corresponds approximately to 5 by 5 by 4 grid cells. In the presence of strong shear in the flow, this opens up the possibility of high-velocity variability in model predictions that will not be captured in the ADV measurements. Thus the average, standard deviation and range of model predictions corresponding to each ADV measurement location were determined.

3.7. Numerical Experiments

[28] Following from model validation, a series of experiments were undertaken to assess the interaction between topographic data density and flow field representation, for a given mesh design. They also sought to address the influence of a range of boundary conditions, notably the free surface treatment and roughness height.

4. Results: Validation

[29] Figure 7 shows a comparison of vertical variation of the downstream variation of velocity above the bed for eight velocity profiles, four from each of rows B and D in Figure 5, closest to the downstream end of the simulation. The results are extremely encouraging. First, and most importantly as compared with previous experiments [e.g., *Nicholas*, 2001], the model is especially effective at predicting strong shear, generally between 0.1 and 0.2 z/h above the bed. Although this study differs from that of *Nicholas* [2001] in that we do not ensemble model predictions and field data but consider velocity profiles at specific locations, *Nicholas* [2001] found that a wall function approach failed to reproduce the shear because: (1) the necessary roughness height required excessively coarse mesh sizes at the bed, reducing resolution of the variation of velocity with elevation above the bed; and (2) the wall function does not represent the larger clasts that protrude into the flow. The porosity approach deals with both of these problems in that it allows application of the wall function to be restricted to grain-scale roughness, permitting much finer grid cells at the bed. When coupled to the specification of the bed using high-resolution digital photogrammetry, it also allows representation of the influence of downstream variation in elevation associated with protruding clasts, and hence reproduces both situations where high velocities extend to the bed at the top of protruding clasts and where there is flow separation, both upstream and downstream of large particles.

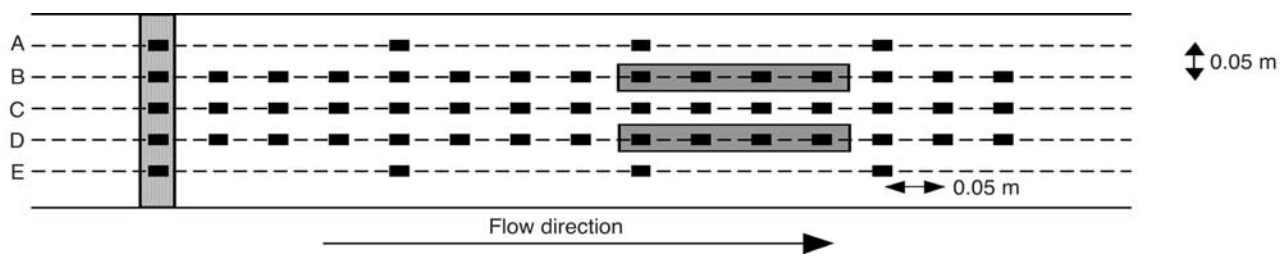

Figure 5. The planform positions where the ADV was used to obtain vertical profiles. The inlet conditions in Figure 6 were determined from data collected from the stippled area. The velocity profiles shown in Figure 7 are taken from the shaded area.

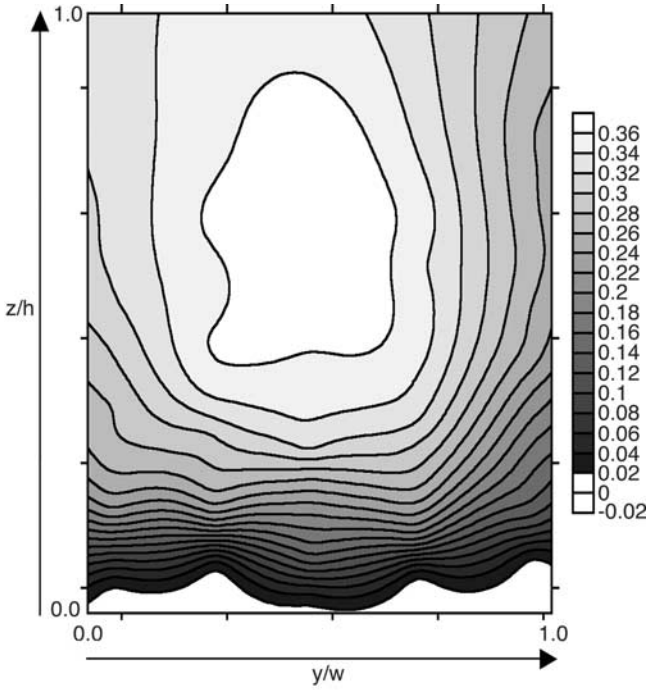

Figure 6. An example inlet condition (for downstream velocity) used to initialize the model.

[30] Figure 8 shows a comparison of model predictions and field measurements for the downstream and vertical components of velocity, and Table 2 shows the associated levels of explanation as compared with previous studies. As *Lane and Richards* [2001] note, there is a poor tradition of using formal statistical evaluations of the agreement between model predictions and field measurements and a tendency to focus upon qualitative comparisons of the vertical variation of downstream velocity with elevation above the bed [e.g., *Czernuszenko and Rylov*, 2000; *Meselhe and Sotiropolous*, 2000; *Sanjiv and Marelius*, 2000; *Sofialidis and Prinos*, 2000; *Huang et al.*, 2002]. This is why Table 2 only covers a selected range of application of 3-D CFD models to river channel problems. In terms of flow speed, results from this study are similar to those obtained by *Hodskinson and Ferguson* [1998] but considerably better than those obtained by other authors. When flow speed is disaggregated into three orthogonal flow components, previous models are found to perform less well [*Lane et al.*, 1999]. In this case, the model retains a good agreement in terms of downstream velocity (Table 2) and matches that obtained with a laboratory study [*Bradbrook et al.*, 1998] involving a smooth bed, but complex flow separation associated with a tributary. The agreement with vertical velocity is less good, but commensurate with that obtained for laboratory studies with smooth beds [e.g., *Bradbrook et al.*, 2001]. This is partly to be expected given the smaller range of magnitude of vertical velocities.

[31] The level of correspondence implied in Table 2 and Figure 8 is also affected by the difference in the spatial scale over which laboratory measurements are made as compared with the model grid size. As noted above, the ADV measurement volume corresponds to approximately 100 grid cells. Figure 7 shows extremely strong velocity gradients at the bed and it is here that the effect of this resolution difference would be most acutely noted. Figure 9a shows the squared error in downstream and vertical velocities against relative elevation above the local bed, showing that the larger errors are generally found closer to the bed. Figure 9b shows that the standard deviation of model predictions within a given ADV measurement volume is significantly greater at the bed. This confirms that much of the error dependence in Figure 9a must partly arise from strong shear at the bed within the

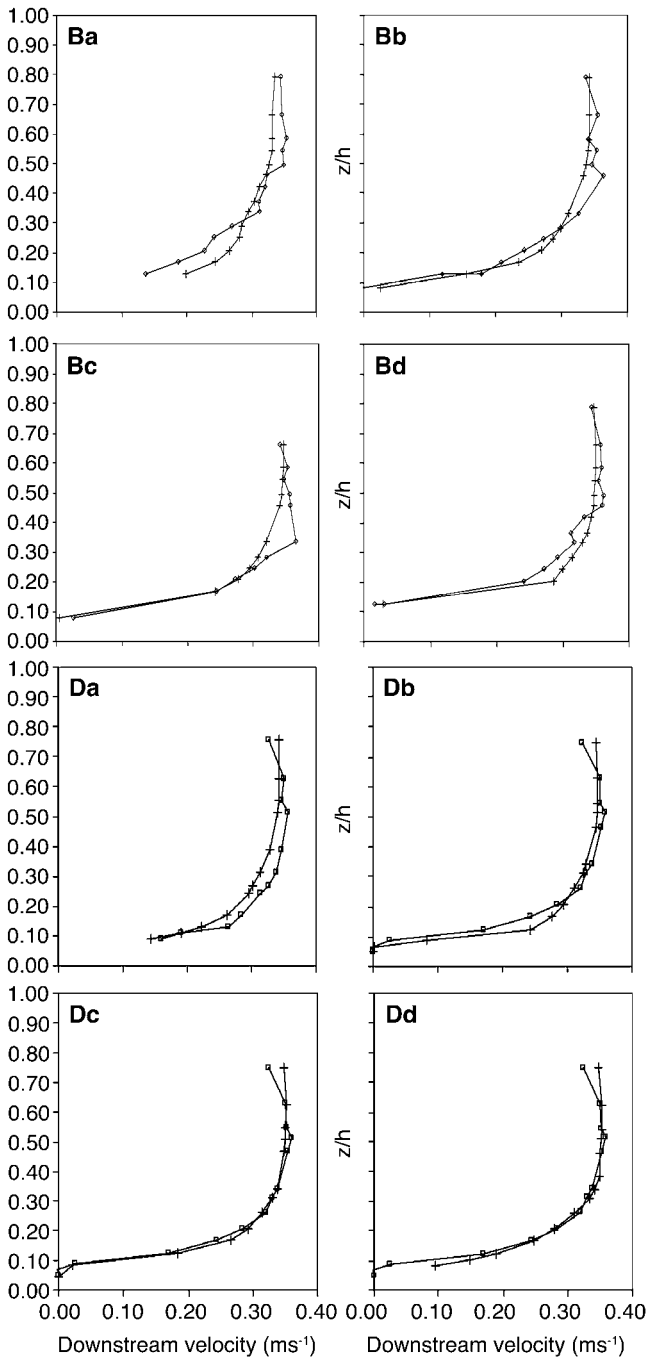

Figure 7. Comparison of predicted downstream velocity profiles with those measured using the ADV. Profiles Ba to Bd refer to row B in Figure 5. Profiles Da to Dd refer to row D in Figure 5. Crossed markers are predicted velocities.

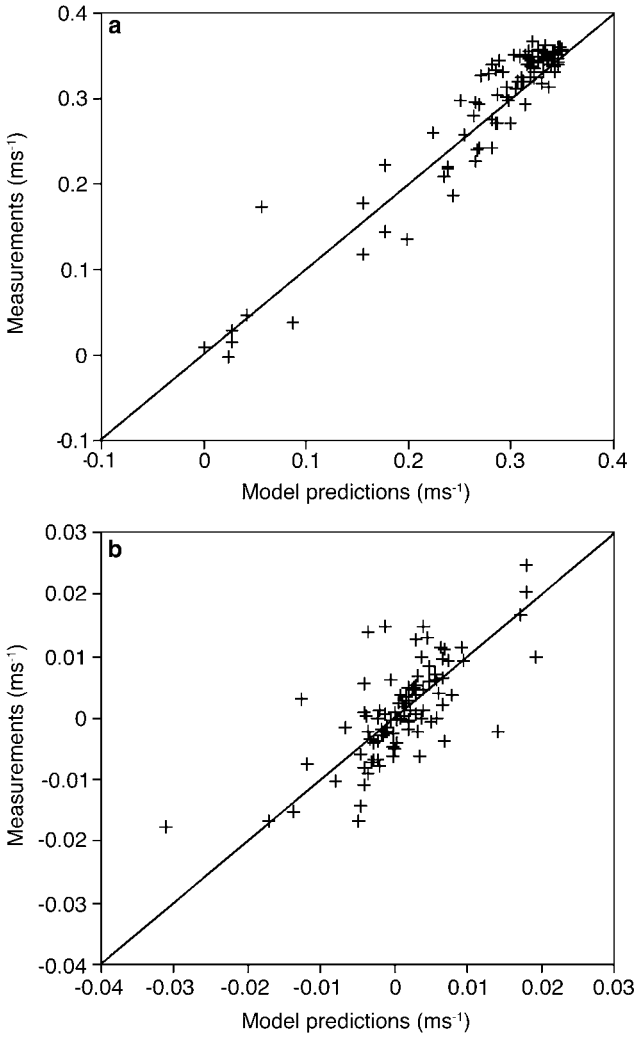

Figure 8. Comparison of a random sample of model predictions and ADV measurements for (a) downstream and (b) vertical flow components. The diagonal is the line of equality.

measurement volume and it is probable that the results in Table 2 and Figure 8 underestimate the quality of model predictions.

5. Results: Numerical Experiments

[32] Figure 10 shows a comparison of model predictions for downstream and vertical velocity and turbulent kinetic energy (tke) with a smooth boundary (i.e., equation (2a)) and a 0.002 m roughness height. Figures 10a–10c are direct comparisons, but standardized with respect to the maximum velocity/tke recorded. These results are important as they demonstrate that the effect of the law of the wall is strongly limited to the grid cells nearest to the bed: inspection of the data used to generate Figure 10 shows that standardized changes are less than 1% of the maximum recorded value except in the wall cells over a range equivalent to $0 < z/h < 0.05$ immediately above each wall cell. As expected, the magnitudes of velocity sensitivity (scales in Figures 10a and 10b) are an order of magnitude less than the tke sensitivity (scales in Figure 10c) and the latter extends marginally higher into the flow. Even with a much finer mesh and topographic resolution, the turbulence associated with sub grid-scale topographic variability is sufficient to create an additional momentum sink as compared with the smooth bed case. However, the spatially restricted nature of this influence and the relatively low magnitude, demonstrates how the influence of roughness height is small and restricted to the bed: as hypothesized there is significantly reduced dependence of model predictions upon roughness height specification except in the immediate near-bed region.

[33] If we repeat this simulation, but replace the spatial dependence of elevation with a spatially uniform elevation, still represented through a porosity field (i.e., with a spatially uniform set of porosity values), we can demonstrate the effect of grains and grain organizations upon the flow (Figure 11). The dashed line shows the spatially averaged elevation. The largest differences are where points on the centerline of the flume experiment either contain gravel in the true topography (above the dashed line and which become "unblocked" when a spatially averaged elevation is used) or do not contain gravel in the true topography (below the dashed line and which become "blocked" when a spatially averaged elevation is used.). For the downstream component (Figure 11a), there are some discernible differences immediately above these blocked and unblocked areas. However, the sensitivity of the vertical flow component to topographic specification is much greater (Figure 11b) than the downstream component. This implies limits to the predictability of vertical fluid flow components over gravely surfaces in the absence of high-resolution topographic representation. Comparison with Figures 10 and 10b suggests that both u and w are more sensitive to topographic specification than roughness specification. It also emphasizes the difficulty of treating both undetermined and indeterminate topographic variability through a roughness height, even if this is allowed to vary spatially. The effects upon turbulent kinetic energy (Figure 11c) mirror the downstream component of velocity given that gradients in u will be the prime source of turbulence in a model like this. It should be noted that these findings need to be re-evaluated with either a turbulence model that can predict the effects of turbulence anisotropy or a Large Eddy Simulation, as it is possible that with the full topographic representation, the turbulence will extend much further into the flow.

[34] These simulations are summarized, along with the other numerical experiments undertaken, in Figure 12. Here we assess the effects of different boundary conditions and topographic data upon the spatially averaged downstream flux. This is taken as a measure of the intensity of secondary circulation: as the downstream flux is reduced, progressively greater proportions of downstream flow are being converted into cross-stream and vertical velocities. A number of interesting points emerge. First, in this scheme, the smooth bed treatment (i.e., equation (2a)) actually results in a lower downstream flux than the default case. This is initially surprising as the switch to a smoother bed might be expected to increase the downstream flux. However, the smooth bed will allow the topography represented in the model to have a greater effect on the boundary flow, and hence increase the magnitude of cross-stream and vertical flows. This would

Table 2. Previous Applications of Three-Dimensional CFD to Natural River Channels in Which a Quantitative Assessment of Model Predictions Has Been Undertaken[a]

Source	Description of Study	Flow Speed	Downstream Velocity	Vertical Velocity
This study	experimental study of channel with rough bed	0.91	0.91	0.51
Bradbrook et al. [1998]	laboratory study of a tributary junction with parallel tributaries; a step was present in one of the tributaries and the bed was smooth	not reported	0.95	0.75
Hodskinson and Ferguson [1998]	field study of a sharp meander bend with flow separation; D_{84} = 0.066 m	0.89	not reported	not reported
Lane et al. [1999]	field study of a tributary junction in a gravel bed river; the bed was rough with D_{50} = 0.050 m	not reported	0.50	0.25
Nicholas and Sambrook-Smith [1999]	field study of flow around a gravel bar in a braided river; rough bed with D_{50} = 0.086 m	0.78	not reported	not reported
Booker et al. [2001]	field study of a riffle-pool sequence. Rough bed with D_{50} = 0.019 m	0.77	not reported	not reported
Bradbrook [2000]	field study of a tributary junction in a sand-bed river; the bed was rough due to sand bed forms with D_{50} = 0.050 m	not reported	0.50	0.01
Bradbrook et al. [2001]	laboratory study of a tributary junction angled at 30° degree to the post-tributary channel; a step was present in the angled tributary and the bed was smooth	not reported	0.53	0.59

[a]Values given are for R^2 (the coefficient of variation obtained, generally using ordinary least squares regression between model predictions and field or laboratory observations).

serve to reduce the downstream flux. This explains the observation made by *Nicholas* [2001] that roughness length scales could be considerably reduced when a randomly perturbed bed replaced a uniform bed in a two-component (downstream and vertical velocity) model of flow over a gravelly surface. In 2-D and 3-D flow models, roughness heights do not effectively represent the blockage effect of spatial variability in bed elevation. The latter creates substantial vertical and cross-stream velocities that can have a major flux. Second, the model displays negligible sensitivity to a 50% reduction in roughness height (Figure 12). The introduction of the porosity treatment, coupled to high-quality topographic representation, limits roughness effects to skin friction. Third, creation of a topography with a 0.004 m spacing (essentially smoothing the surface) resulted in the largest change in downstream flux: Smoothing the topography increased downstream flux. Again, changing the nature of the roughness height determination (from rough to smooth, or by reducing the roughness height by 50%) had a negligible effect upon flux as compared with the effects of topographic smoothing. This confirms the observation that roughness height is not an effective parameter for representing the effects of gravel bed topography upon flow processes. Finally, and reflecting the observation that the bed influence is limited to the bottom part of the flow, removing the free surface treatment had negligible effects upon downstream flux.

6. Flow Fields Over Gravelly Surfaces

[35] Figure 13 shows five extracted cross sections of downstream velocity for x/l = 0.488, 0.494, 0.500, 0.506 and 0.512, which corresponds to a 0.004 m spacing in the downstream direction. Figure 13 shows large spatial variation in near-bed downstream velocities, and this is reflected in the difference in the centerline predictions of downstream velocity when they were compared with the spatially averaged porosity (Figure 11a). Over the spatial scale of

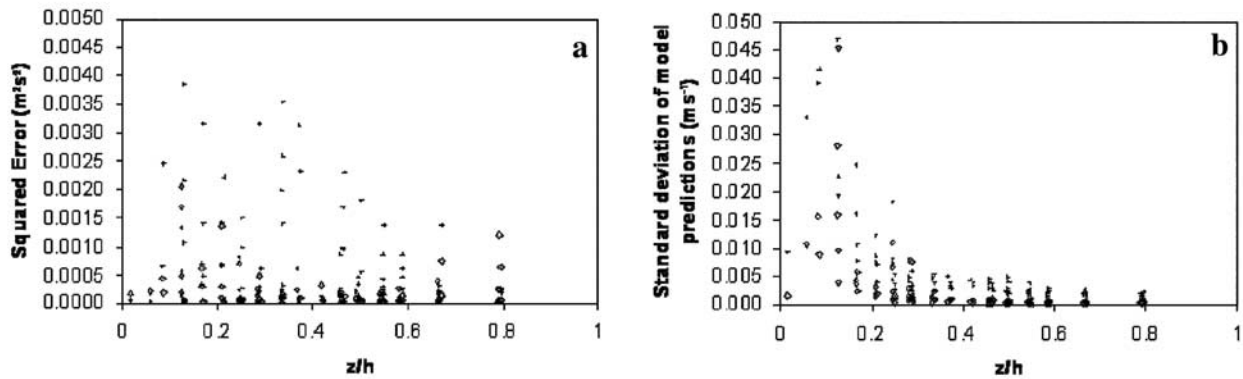

Figure 9. (a) Plot of the squared error in velocity and (b) standard deviation of model predictions estimated to be within a given ADV measurement volume against relative elevation above the local bed. Downstream velocity errors are shown as crosses and vertical velocity errors are shown as diamonds.

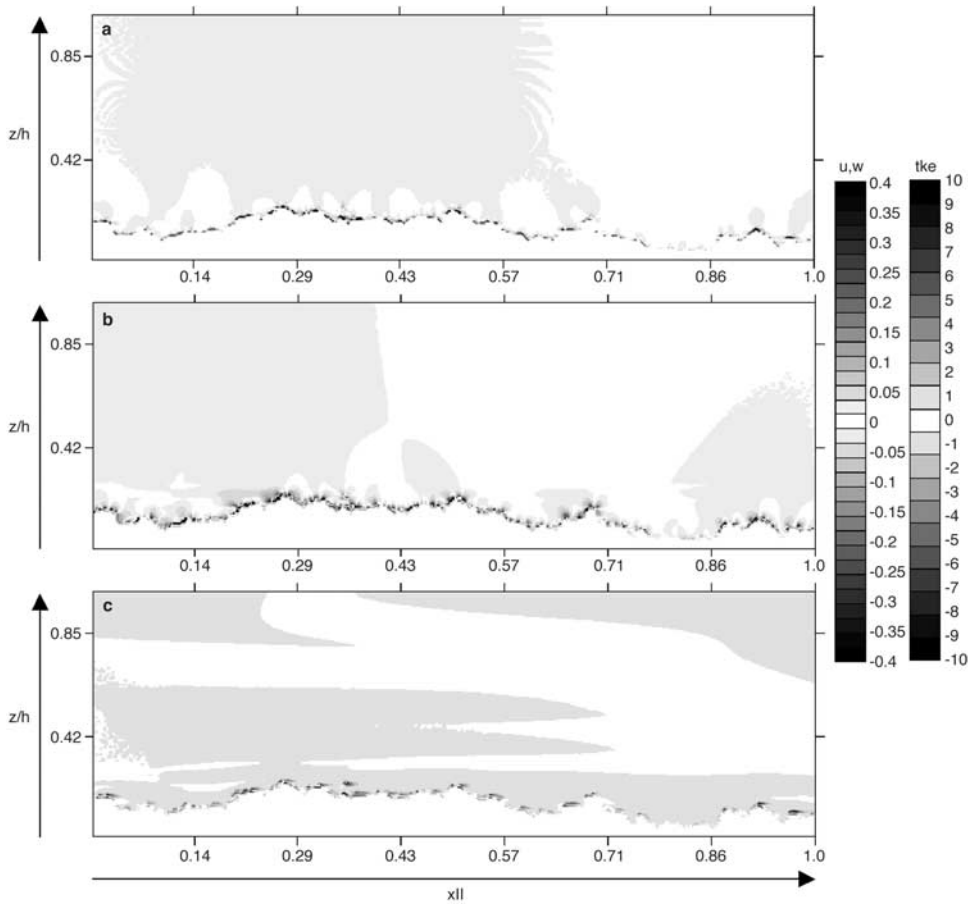

Figure 10. The difference between model predictions with a rough boundary (z_o = 0.002 m) and a smooth boundary, standardized by the maximum velocity/turbulent kinetic energy recorded with the rough boundary. (a) Downstream velocity, (b) vertical velocity, and (c) turbulent kinetic energy per unit mass. Note the plots show little change as the effects of z_o are restricted to the bed.

model predictions in Figure 13, there is little variation in downstream velocity away from the boundary. However, the five cross sections describe flow around a large particle, located at y/w = 0.6 in Figure 14c. Upstream of x/l = 0.5, there is upwelling around this particle (Figures 14a and 14b), which is strongest at x/l = 0.494 (Figure 14b). At this point, there is also a weak stagnation point, with a zone of very slow downstream velocity (Figure 13b) and a steep velocity gradient above this. This stagnation has been observed in flume studies of flow around idealized objects (e.g., M. Lawless et al., The effects of obstacle size and shape upon the time-averaged juncture vortex: An experimental study, submitted to *Journal of Fluid Mechanics*, 2003) (hereinafter referred to as Lawless et al., submitted manuscript, 2003) and is commonly associated with a juncture vortex. By x/l = 0.5, the core of high velocity extends almost to the top of the particle (Figures 13c and 13d) and the magnitude of upwelling is reduced (Figures 14c and 14d). This is associated with the highest point on the protruding particle. Downstream of this, the velocity gradient is reduced (Figure 13e) and there is strong downwelling in the lee of the particle (Figure 14e). Figures 13 and 14 both demonstrate that the influence of topographic variability at the bed is limited to essentially the bottom 25% of the flow. Vertical velocities approach approximately 40% of the maximum downstream velocity and are primarily associated with locations of high rates of topographic change, upstream and downstream of particles. These are significantly higher than the secondary circulations that have been measured in straight channels associated with turbulence anisotropy [e.g., *Nezu and Nakagawa*, 1993] but, unlike observations of macroturbulent flow structure over gravel surfaces [e.g., *Buffin-Belanger et al.*, 2000; *Shvidchenko and Pender*, 2001] they are restricted to the bed, generally the bottom 5% of the flow which corresponds to *c.* 0.010 m. This emphasizes the challenge (see Table 1 and Figure 9) of validating model predictions in this case as this range is similar to the vertical extent of the ADV measuring volume (0.008 m). It is probable that our ability to model this flow zone now exceeds our ability to measure it, except using the new generation of particle image velocimeters (e.g., Lawless et al., submitted manuscript, 2003).

[36] Figure 15 shows predictions of turbulent kinetic energy per unit mass (k) for a long-section. This shows two important features. First, there are very high values of k close to the bed, again in a zone where there is most uncertainty in terms of ADV measurement. It has traditionally been assumed that this is a zone of much lower values of k as a result of damping of streamwise turbulence intensities in the lee of roughness elements [e.g., *Nezu*

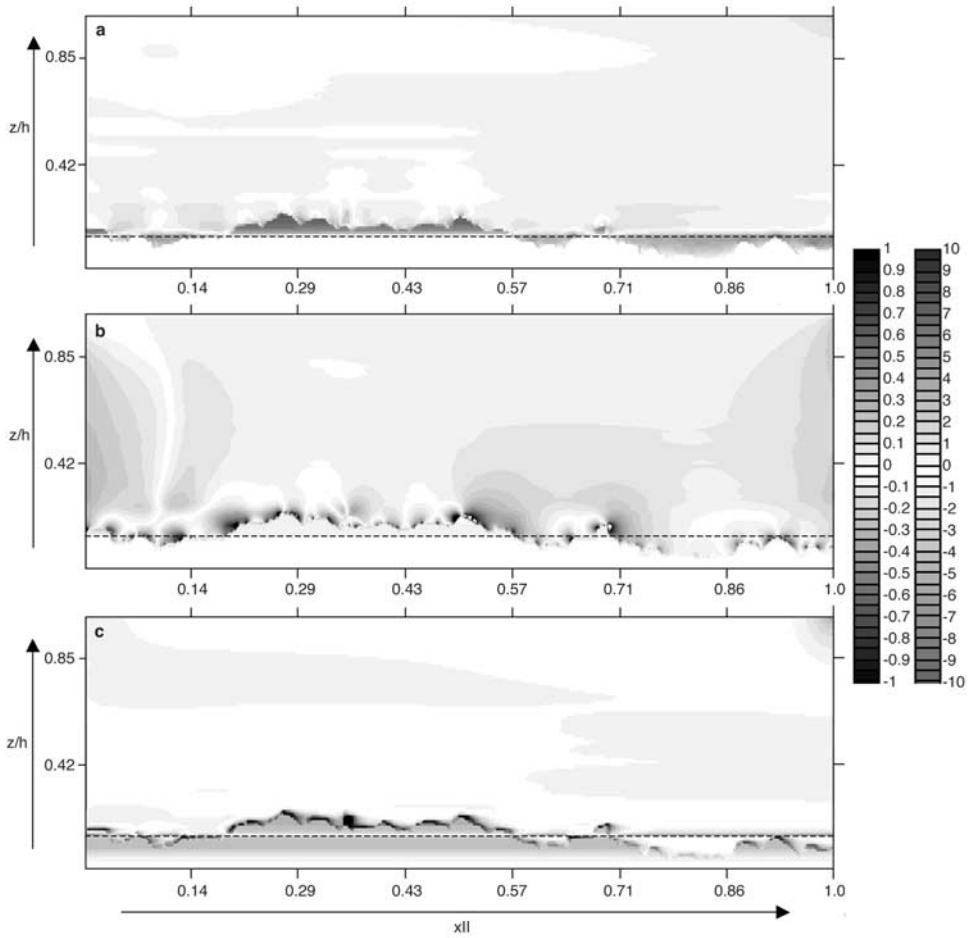

Figure 11. The difference between model predictions with a full topographic representation and a spatially uniform elevation with the porosity values set so that the volume of bed occupied is the same as with the full topographic representation. The boundary is set as rough (z_o = 0.002 m). Predictions are standardized by the maximum velocity/turbulent kinetic energy recorded with the rough boundary. (a) Downstream velocity, (b) vertical velocity, and (c) turbulent kinetic energy per unit mass. The dashed line shows the elevation of the spatially averaged porosity field.

and Nakagawa, 1993; *Nicholas*, 2001]. This is evident in Figure 15 (e.g., at x/l = 0.71), but the effects of particle protrusion into the flow result in three-dimensional flow separation, resulting in generally high values of k at the bed, notably where particles extend into the flow.

[37] Second, there is a zone of higher k at about z/h = 0.20, associated with the zone of maximum shear in the vertical variation of downstream velocity with elevation above the bed. This zone has been observed before, both in measurements [e.g., *Wang et al.*, 1993] and model predictions [e.g., *Nicholas*, 2001], although at a somewhat lower relative elevation above the bed (z/h = 0.10 to 0.15). In this case, we define z with reference to the lowest elevation in the DEM, which will serve to raise the value of z/h at which the high k zone would be found. This is the well-established problem of determining a reference height when the surface varies in a complex way. However, when considering somewhat larger roughness elements, *Lawless and Robert* [2001] identified peak k values between $0.33 < z/h < 0.50$ into the flow, associated with a shear layer in the flow. Inspection of u component velocity predictions from the model identifies a zone of strong shear coincident with the

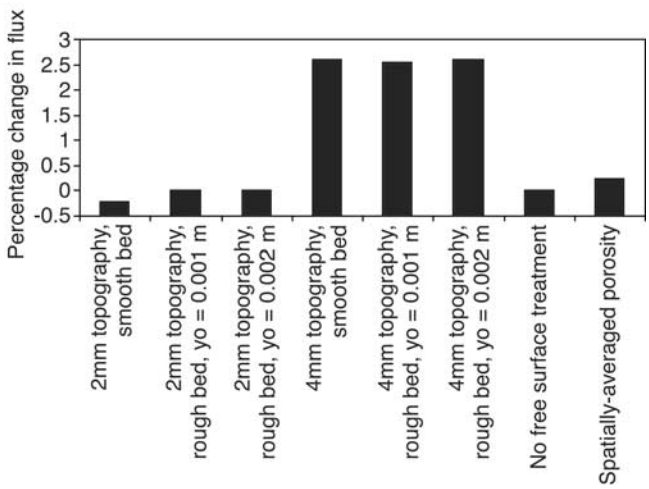

Figure 12. The percentage change in average downstream flux with different numerical treatments as compared with the default case (a 0.002 m topographic data spacing with a 0.002 m roughness height).

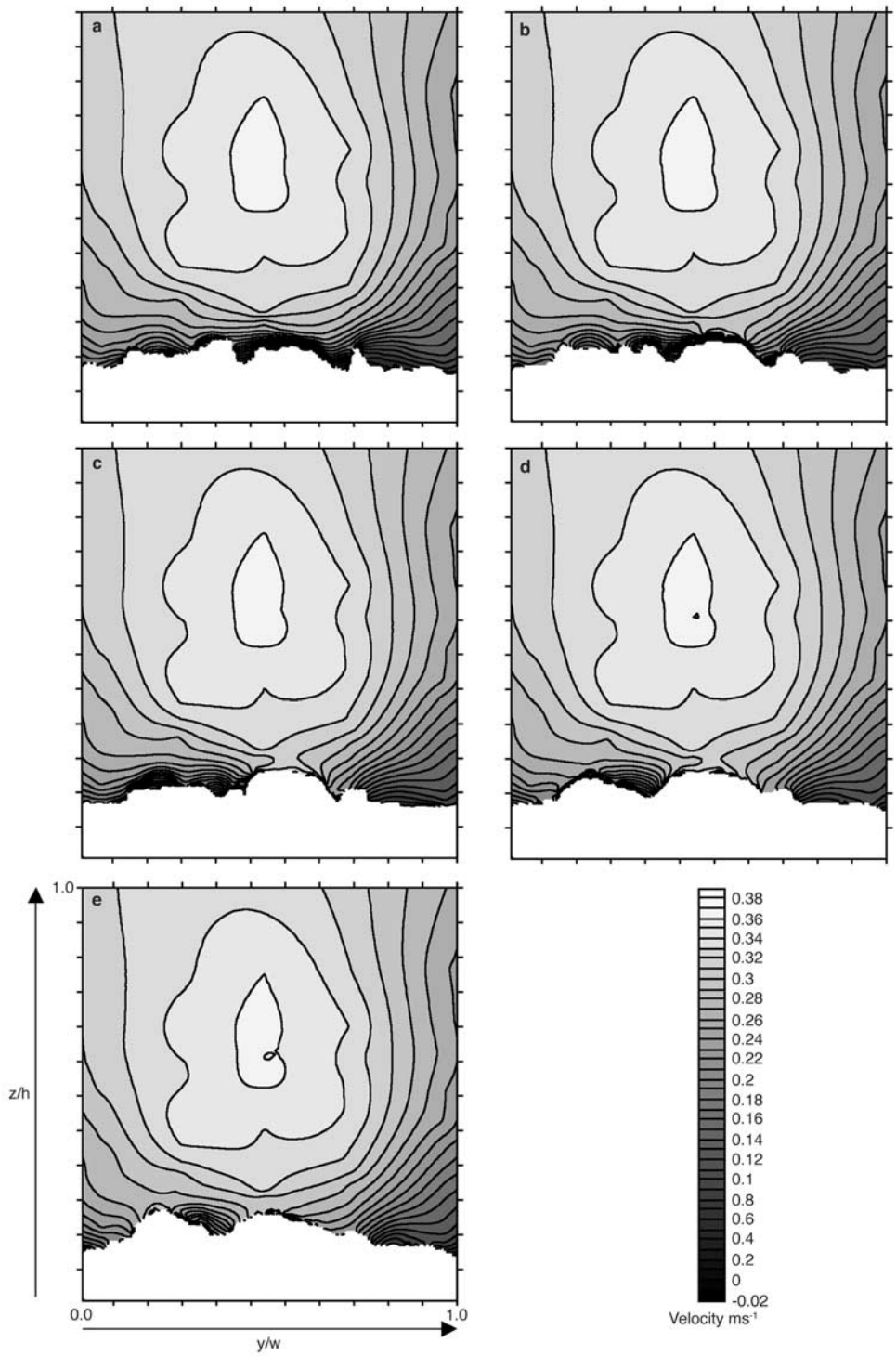

Figure 13. Downstream velocity plots for cross sections at x/l = (a) 0.488, (b) 0.494, (c) 0.500, (d) 0.506, and (e) 0.512, corresponding to a 0.004 m spacing.

peak k values, at an elevation controlled by the height of the particles that protrude farthest into the flow. This matches directly the observations of *Buffin-Belanger and Roy* [1998] and *Lawless and Robert* [2001] that the largest obstacles in a gravel bed create strong shear at the crest of the obstacle that can have strong downstream provenance both because of the magnitude of shear created and because the shear is not affected by obstacles further downstream. In turn, this explains the high values of k at the bed, where the continuous variation of bed topography creates extensive shear in the bottom part of the flow as compared with the traditional damping of turbulent kinetic energy expected with decreasing distance from a smooth bed.

[38] The main limiting issue in this study relates to the turbulence model being used in this study. A number of researchers have described depth-scale flow structures over gravelly beds [e.g., *Buffin-Belanger et al.*, 2000; *Shvidchenko and Pender*, 2001], including time-varying

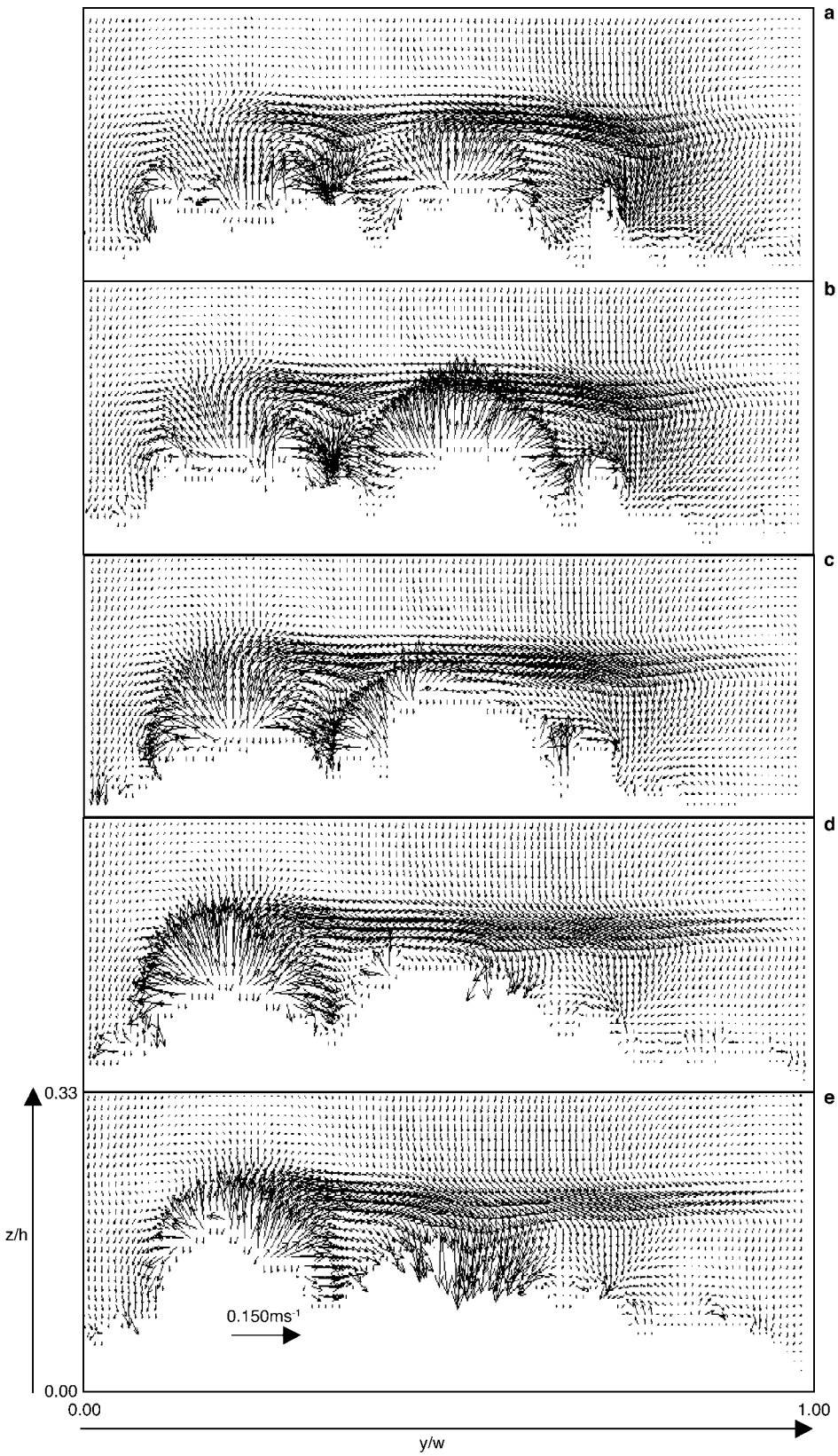

Figure 14. Predicted velocity vectors for cross sections at x/l = (a) 0.488, (b) 0.494, (c) 0.500, (d) 0.506, and (e) 0.512, corresponding to a 0.004 m spacing.

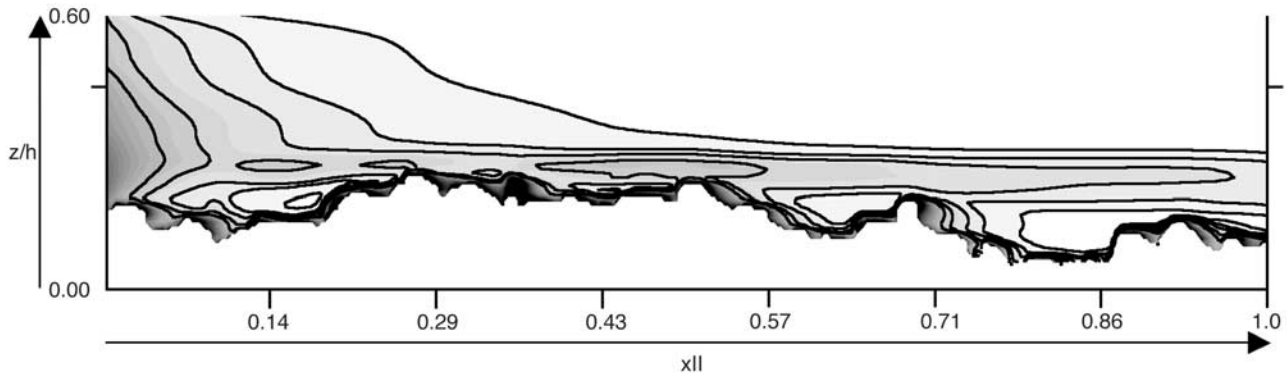

Figure 15. Turbulent kinetic energy per unit mass (m^{-2} s^{-2}) extracted along the centerline of the flume (i.e., $y/w = 0.5$).

low speed and high-speed regions [e.g., *Kirkbride and Ferguson*, 1995; *Buffin-Belanger et al.*, 2000]. *Shvidchenko and Pender* [2001] observe that these may be associated with large-scale eddies with a vertical extent associated with the flow depth, and which migrate downstream. Clearly, a time-averaged turbulence model will encounter severe problems in reproducing this type of flow structure, despite its clear importance for sediment transport [e.g., *Shvidchenko and Pender*, 2001]. Even if a turbulence model, that is capable of modeling the effects of anisotropic turbulence upon mean flow parameters [e.g., a Reynolds Stress Model), were to be used, it is highly unlikely that these relatively low period velocity fluctuations would be reproduced in a time-averaged flow field. Thus current research is applying Large Eddy Simulation to the quantification of time-dependent flow structures.

7. Implications and Applications

[39] A number of important substantive implications emerge from this research. First it has demonstrated the nature of bed topographic forcing associated with individual clasts, which was found to be restricted to the bottom 25% of the flow, but which could approach 40% of the downstream flow velocity. This magnitude of variability will dwarf any secondary circulations caused by other processes, such as turbulent anisotropy, and this suggests that vertical flow variability in gravel bed rivers are topographically driven, rather than hydrodynamically driven. However, it should be emphasized that the results are from a time-averaged solution: time-dependent eddy shedding may extend to the full flow depth [e.g., *Shvidchenko and Pender*, 2001] and interaction with the water surface should be expected. Second, it shows that the position of maximum shear is pinned by the elevation of the top of the most protruding particles. The larger particles are associated with greater bed separation, and this appears to enhance turbulent kinetic energy production, rather than damping it right at the bed, as might be expected in smooth channels.

[40] In methodological terms, a number of points emerge. First, the research causes us to be critical of some of the existing research [e.g., *Lane et al.*, 1999; *Bradbrook et al.*, 2000] into flow structure formation in shallow gravel bed rivers. This is especially the case where the flow is shallow as compared to the bed topographic variance, and experiments are required to assess the effects of different flow depth to surface variance ratios upon the sorts of flow structures that form. The same conclusion applies to estimates of bed shear stress derived from three-dimensional applications of CFD to gravel bed rivers where there is no proper topographic representation. Second, it emphasizes the need for more sophisticated representation of the effects of bed topographic variability upon the flow field. In this case, we dealt with an ideal situation where the bed surface structure had been measured precisely to a high resolution, with the precision and resolution an order of magnitude smaller than the median grain-size of the bed. The techniques used to generate this data can be applied in clear water streams in the field [*Butler et al.*, 2002], although the associated fieldwork needs to be carefully designed. However, it is unlikely to be feasible to acquire this sort of data regularly at the river reach-scale. The solution will be larger-scale mapping of characteristic reach morphology (e.g., riffle-pool morphology) coupled to reconstruction of gravel topography for scales smaller than those mapped. *Butler et al.* [2001] used two-dimensional fractal analysis of water worked gravels to produce characteristic scaling relationships. These can be used to create gravel topography with the same scale-dependent statistical properties and so represent the effects of gravel topography upon reach-scale flow structures, if not the exact detail. A similar approach has been used by *Nicholas* [2001] albeit using a scale-independent estimate of surface variance and boundary-fitted coordinates with a two-dimensional (vertical and downstream) model. The recommended approach is in preference to multiplication upward of roughness lengths as this does not effectively represent blockage effects, and does not pin the position of maximum shear at the right elevation in the vertical. The latter may be crucial for getting the downstream flux to be correct.

[41] The main limitation to applying this development at the reach-scale will be the computational resources required. The approach adopted has the advantage of using regular structured grids in a finite volume formulation which makes it suitable to the new generation of fast numerical solvers. However, even then, using mesh resolutions smaller than 0.01 m at the reach-scale will remain computationally unfeasible for some time. However, the porosity method may be adapted to situations where the reach-scale geometry is complex (e.g., tributary junctions, tight meander

bends with inner or outer bank separation) and obtaining numerically acceptable grids is difficult, even with boundary-fitted coordinates or unstructured grids. This would use the same porosity formulation and drag scaling, although the effects of the latter would become much more important than was found to be the case here. This is an area for further research. Concurrently, it will have implications for the boundary conditions required for initialization of the model (e.g., distributed 3-D flow data at the inlet, water level at the outlet), although methods have been developed for situations where this data is not necessarily available [e.g., *Bradbrook et al.*, 2000]. However, this research emphasizes the importance of a priori measurement of topography, if successful predictions of flow fields are to be derived for gravel bed rivers.

8. Conclusions

[42] This paper has described the development, application and validation of a porosity-based, structured mesh solution of the time-averaged 3-D Navier Stokes equations for gravel bed rivers. This has been based upon using high-resolution measurements of a flume bed, acquired using two-media digital photogrammetry, to specify the bed geometry. Comparison with validation data acquired using an Acoustic Doppler Velocimeter showed an excellent agreement between model predictions and flow measurements given: (1) relatively few studies have previously undertaken quantitative assessment; (2) that good agreement in terms of vertical flow components has only previously been obtained for laboratory studies with smooth beds; and (3) the very effective representation of shear at the bed in the downstream flow velocities. Sensitivity testing revealed very low sensitivity to whether a rough or a smooth bed was used at the wall and to whether or not there was a free surface treatment. Comparison with a spatially averaged bed surface emphasized the limits to prediction associated with vertical velocity components in situations where the bed is not fully specified. Model predictions represented effectively the changing flow field around individual bed particles. This suggested that the most protruding bed particles exerted a critical control on the turbulent kinetic energy maxima typically observed at about 20% of the flow depth above the bed.

[43] **Acknowledgments.** This research was funded by NERC grant GR9/5059 awarded to SNL, LE and DBI. The flume data were acquired by J. Butler, funded by a NERC studentship between 1995 and 1998, and jointly supervised by SNL and J. Chandler.

References

Booker, D. J., D. A. Sear, and A. J. Payne (2001), Modelling three-dimensional flow structures and patterns of boundary shear stress in a natural pool-riffle sequence, *Earth Surf. Processes Landforms*, *26*, 553–576.

Bradbrook, K. F. (2000), Numerical, field and laboratory studies of three-dimensional flow structures at river channel confluences, Ph.D. thesis, 362 pp., Univ. of Cambridge, Cambridge, U. K.

Bradbrook, K. F., P. Biron, S. N. Lane, K. S. Richards, and A. G. Roy (1998), Investigation of controls on secondary circulation and mixing processes in a simple confluence geometry using a three-dimensional numerical model, *Hydrol. Processes*, *12*, 1371–1396.

Bradbrook, K. F., S. N. Lane, and K. S. Richards (2000), Numerical simulation of time-averaged flow structure at river channel confluences, *Water Resour. Res.*, *36*, 2731–2746.

Bradbrook, K. F., S. N. Lane, K. S. Richards, P. M. Biron, and A. G. Roy (2001), Flow structures and mixing at an asymmetrical open-channel confluence: a numerical study, *J. Hydraul. Eng.*, *127*, 351–368.

Bray, D. I. (1982), Flow resistance in gravel-bed rivers, in *Gravel-Bed Rivers*, edited by R. D. Hey, J. C. Bathurst, and C. R. Thorne, pp. 109–133, John Wiley, Hoboken, N. J.

Buffin-Belanger, T., and A. G. Roy (1998), Effects of a pebble cluster on the turbulent structure of a depth-limited flow in a gravel-bed river, *Geomorphology*, *25*, 249–267.

Buffin-Belanger, T. A., A. G. Roy, and A. D. Kirkbride (2000), On large-scale flow structures in a gravel-bed river, *Geomorphology*, *32*, 417–435.

Butler, J. B., S. N. Lane, and J. H. Chandler (1998), Assessment of DEM quality for characterising surface roughness using close range digital photogrammetry, *Photogramm. Rec.*, *16*, 271–291.

Butler, J. B., S. N. Lane, and J. H. Chandler (2001), Application of two-dimensional fractal analysis to the characterisation of gravel-bed river surface structure, *Math. Geol.*, *33*, 301–330.

Butler, J. B., S. N. Lane, J. H. Chandler, and K. Porfiri (2002), Through-water close-range digital photogrammetry in flume and field environments, *Photogramm. Rec.*, *17*, 419–439.

Chandler, J. H., K. Shiono, P. Rameshwaren, and S. N. Lane (2001), Automated DEM extraction for hydraulics research, *Photogramm. Rec.*, *17*, 39–61.

Clifford, N. J., A. Robert, and K. S. Richards (1992), Estimation of flow resistance in gravel-bedded rivers: A physical explanation of the multiplier of roughness length, *Earth Surf. Processes Landforms*, *17*, 111–126.

Cornelius, C., W. Volgmann, and H. Stoff (1999), Calculation of three-dimensional turbulent flow with a finite volume multigrid method, *Int. J. Numer. Methods Fluids*, *31*, 703–720.

Crowder, D. W., and P. Diplas (2000), Evaluating spatially explicit metrics of stream energy gradients using hydrodynamic model simulations, *Can. J. Fish. Aquat. Sci.*, *57*, 1497–1507.

Crowder, D. W., and P. Diplas (2002), Assessing changes in watershed flow models with spatially explicit hydraulic models, *J. Am. Water Resour. Assoc.*, *38*, 397–408.

Czernuszenko, W., and A. A. Rylov (2000), A generalisation of Prandtl's model for 3D open channel flows, *J. Hydraul. Res.*, *38*, 133–139.

Dietrich, W. E. (1987), Mechanics of flow and sediment transport in river bends, in *River Channels: Environment and Process*, *Inst. Br. Geogr. Spec. Publ.*, vol. 18, edited by K. S. Richards, pp. 179–227, Blackwell, Malden, Mass.

Gessler, D., B. Hall, M. Spasojevic, F. Holly, H. Pourtaheri, and N. Raphelt (1999), Application of 3D mobile bed, hydrodynamic model, *J. Hydraul. Eng.*, *125*, 737–749.

Hardy, R. J., S. N. Lane, R. I. Ferguson, and D. Parsons (2003), Assessing the credibility of a series of computational fluid dynamic (CFD) simulations of open channel flow, *Hydrol. Processes*, in press.

Hey, R. D. (1979), Flow resistance in gravel-bed rivers, *J. Hydraul. Div. Am. Soc. Civ. Eng.*, *105*, 365–379.

Hodskinson, A., and R. I. Ferguson (1998), Numerical modelling of separated flows in river bends: Model testing and experimental investigation of geometrical controls on the extent of flow separation at the concave bank, *Hydrol. Processes*, *11*, 1323–1338.

Huang, J. C., L. J. Weber, and Y. G. Lai (2002), Three-dimensional numerical study of flows in open-channel junctions, *J. Hydraul. Eng.*, *128*, 268–280.

Kirkbride, A. D., and R. I. Ferguson (1995), Turbulent flow structure in a gravel-bed river: Markov chain analysis of the fluctuating velocity profile, *Earth Surf. Processes Landforms*, *20*, 721–733.

Lane, S. N. (1998), Hydraulic modelling in hydrology and geomorphology: A review of high resolution approaches, *Hydrol. Processes*, *12*, 1131–1150.

Lane, S. N. (2001), The measurement of gravel-bed river morphology, in *Gravel-Bed Rivers V*, edited by M. P. Mosley, pp. 291–320, N. Z. Hydrol. Soc., Wellington.

Lane, S. N., and K. S. Richards (2001), The "validation" of hydrodynamic models: Some critical perspectives, in *Model Validation for Hydrological and Hydraulic Research*, edited by P. D. Bates and M. G. Anderson, pp. 413–438, John Wiley, Hoboken, N. J.

Lane, S. N., P. M. Biron, K. F. Bradbrook, J. B. Butler, J. H. Chandler, M. D. Crowell, S. J. McLelland, K. S. Richards, and A. G. Roy (1998), Integrated three-dimensional measurement of river channel topography and flow processes using acoustic Doppler velocimetry, *Earth Surf. Processes Landforms*, *23*, 1247–1267.

Lane, S. N., K. F. Bradbrook, K. S. Richards, P. M. Biron, and A. G. Roy (1999), The application of computational fluid dynamics to natural river channels: Three-dimensional versus two-dimensional approaches, *Geomorphology*, *29*, 1–20.

Lane, S. N., K. F. Bradbrook, K. S. Richards, P. M. Biron, and A. G. Roy (2000), Secondary circulation in river channel confluences: Measurement myth or coherent flow structure?, *Hydrol. Processes*, *14*, 2047–2471.

Launder, B. E., and D. B. Spalding (1974), The numerical computation of turbulent flows, *Comput. Methods Appl. Mech. Eng.*, *3*, 269–289.

Lawless, M., and A. Robert (2001), Three-dimensional flow structure around small-scale bedforms in a simulated gravel-bed environment, *Earth Surf. Processes Landforms*, *26*, 507–522.

Leclerc, M., A. Boudreault, J. A. Bechara, and G. Corfa (1995), Two-dimensional hydrodynamic modelling: A neglected tool in the instream flow incremental methodology, *Trans. Am. Fish. Soc.*, *124*, 645–662.

Leclerc, M., A. Boudreault, J. A. Bechara, and L. Belzile (1996), Numerical method for modelling spawning habitat dynamics of landlocked salmon, *Salmo salar, Reg. Riv. Res. Manage.*, *12*, 273–285.

Manson, J. R., and S. G. Wallis (1997), Accuracy characteristics of traditional finite volume discretizations for unsteady computational fluid dynamics, *J. Comput. Phys.*, *132*, 149–153.

Meselhe, E. A., and F. Sotiropolous (2000), Three-dimensional numerical model for open-channels with free surface variations, *J. Hydraul. Res.*, *38*, 115–121.

Nezu, I., and H. Nakagawa (1993), *Turbulence in Open Channel Flows*, A. A. Balkema, Brookfield, Vt.

Nicholas, A. P. (2001), Computational fluid dynamics modelling of boundary roughness in gravel-bed rivers: An investigation of the effects of random variability in bed elevation, *Earth Surf. Processes Landforms*, *26*, 345–362.

Nicholas, A. P., and G. H. Sambrook-Smith (1999), Numerical simulation of three-dimensional flow hydraulics in a braided channel, *Hydrol. Processes*, *13*, 913–929.

Nikuradse, J. (1933), Laws for flows in rough pipes (in German), *NACA Tech. Memo., 1292*, 62 pp.

Olsen, N. R. B., and S. Stokseth (1995), Three-dimensional numerical modelling of water flow in a river with large bed roughness, *J. Hydraul. Res.*, *33*, 571–581.

Patankar, S. V., and D. B. Spalding (1972), A calculation procedure for heat, mass and momentum transport in three-dimensional parabolic flows, *Int. Heat Mass Transfer, J.*, *15*, 1787–1806.

Prandtl, L. (1952), *Essentials of Fluid Dynamics*, Blackie, London.

Sanjiv, S. K., and F. Marelius (2000), Analysis of flow past submerged vanes, *J. Hydraul. Res.*, *38*, 65–71.

Shvidchenko, A., and G. Pender (2001), Macroturbulent structure of open-channel flow over gravely beds, *Water Resour. Res.*, *37*, 709–719.

Sinha, S. K., F. Sotiropoulos, and A. J. Odgaard (1998), Three-dimensional numerical model for flow through natural rivers, *J. Hydraul. Eng.*, *124*, 13–24.

Sofialidis, D., and P. Prinos (2000), Turbulent flow in open channels with smooth and rough floodplains, *J. Hydraul. Res.*, *37*, 615–640.

Wang, J., C. Chen, Z. Dong, and Z. Xia (1993), The effects of bed roughness on the distribution of turbulent intensities in open channel flow, *J. Hydraul. Res.*, *31*, 89–98.

Whiting, P. J., and W. E. Dietrich (1990), Boundary shear stress and roughness of mobile alluvial beds, *J. Hydraul. Eng.*, *116*, 1495–1511.

Wiberg, P. L., and J. D. Smith (1991), Velocity distribution and bed roughness in high gradient streams, *Water Resour. Res.*, *27*, 825–838.

Wu, W. M., S. S. Y. Wang, and Y. F. Jia (2000), Nonuniform sediment transport in alluvial rivers, *J. Hydraul. Res.*, *38*(6), 427–434.

L. Elliott and D. B. Ingham, Centre for Computational Fluid Dynamics and Department of Applied Mathematics, University of Leeds, Leeds LS2 9JT, UK.

R. J. Hardy and S. N. Lane, School of Geography, Faculty of Earth and Environment, University of Leeds, Leeds LS2 9JT, UK. (s.lane@geog.leeds.ac.uk)